Title: Effect of compressive residual stress introduced by cavitation peening and shot peening on the improvement of fatigue strength of stainless steel

Author: Hitoshi Soyama[*,1] Christopher R. Chighizola[2] and Michael R. Hill[2]

1 Department of Finemechanics, Tohoku University, 6-6-01 Aoba, Aramaki, Aoba-ku, Sendai 980-8579, Japan

2 Department of Mechanical and Aerospace Engineering, University of California Davis, Bainer Hall Drive, Davis, California, 95616, USA

[*] corresponding author.

e-mail address: soyama@mm.mech.tohoku.ac.jp (H. Soyama)

Submitted to Journal of Materials Processing Technology;
Accepted and Published online August 2020, https://doi.org/10.1016/j.jmatprotec.2020.116877

Abstract

One of the traditional methods used to improve the fatigue properties of metallic materials is shot peening. More recently, cavitation peening, in which the surface is treated using cavitation impact, has been developed, and the improvements this makes to the fatigue life and the strength of metallic materials have been reported. In order to clarify the difference between these two methods, stainless steel SUS316L samples were treated by shot peening and cavitation peening, and the fatigue properties of the samples were evaluated utilizing a displacement controlled plane bending fatigue test. The residual stress and hardness before and after the fatigue test were measured, and the surface roughness of each specimen was also measured. It was concluded that the fatigue life of shot peened specimens at bending stress $\sigma_a > 450$ MPa was longer than that of cavitation peened specimens; however, the fatigue strength of the cavitation peened specimens was slightly larger than that of the shot peened specimens. The compressive residual stress introduced by both peening methods decreased during the fatigue test. The reduction in the compressive residual stress in the shot peened specimens was greater than in the cavitation peened specimens, and after the fatigue test, the compressive residual stress in the shot peened specimens was greater than that in the cavitation peened specimens. It was found that the fatigue strength corresponded well with the yield stress estimated from the Vickers hardness corrected by the residual stress obtained after the fatigue test.

Keywords

surface modification; fatigue strength; residual stress; surface roughness; hardness; stainless steel

1. Introduction

One of the effective methods to enhance the fatigue properties of mechanical components comprising polycrystalline metals is shot peening, which introduces compressive residual stress and work hardening. Delosrios et al. (1995) demonstrated that compressive residual stress introduced by shot peening reduced fatigue crack initiation and crack propagation. Wang et al. (1998) proposed an empirical method to estimate the compressive residual stress distribution introduced by shot peening. Torres and Voorwald (2002) investigated the relationship between fatigue life and the compressive residual stress introduced by shot peening. As McClung (2007) surveyed stability of residual stress during fatigue, the relaxation of compressive residual stress introduced by shot peening was reported from 1960's such as for titanium alloy (Leverant et al. (1979)), steel (Torres and Voorwald (2002)) and nickel-based alloy (Foss et al. (2013)). Zhou et al. (2018) considered the residual stress and the relaxation in the residual stress in discussing the fatigue life of shot peened and mechanically treated stainless steel. However, with conventional shot peening the surface roughness increases, as local plastic deformation is required in order to introduce compressive residual stress and work hardening. Bellows and Koster (1972) showed that the fatigue strength decreases as the surface roughness increases. Miao et al. (2010) investigated the relationship between surface roughness and the shot peening processing time up to 100 % coverage, and Bagherifard et al. (2012) showed that the surface roughness increases with shot peening even after 100 % coverage. More recently, a mechanical surface treatment using the impact produced by cavitation bubbles collapsing, i.e., cavitation peening, was proposed and the improvements this makes to the fatigue properties of metallic materials have been reported by Soyama (2017). Takakuwa and Soyama (2012) revealed that cavitation peening suppressed hydrogen embrittlement of stainless steel, and Kumagai et al. showed improvement of delayed fracture resistance on chrome molybdenum steel bolt by cavitation peening. The surface roughness after cavitation peening is less than that after conventional shot peening, as there are no collisions between solids (Soyama and Sekine (2010)). As the processing mechanisms and parameters such as the stress distribution and the strain rate are different for shot peening and cavitation peening, it is worthwhile examining the residual stress and roughness to investigate the fatigue properties arising from shot peening and cavitation peening.

As mentioned above, the compressive residual stress introduced by peening and the relaxation of this stress are important parameters that determine the improvements made to the fatigue properties by mechanical surface treatment. Munoz-Cubillos et al. (2017) considered the residual stress, hardness and surface roughness when investigating the improvements made to the fatigue life of type 304 and 316 stainless steel by deep rolling, and

they concluded that the compressive residual stress introduced by deep rolling was an important factor. Telang et al. (2018) demonstrated that relaxation of the compressive residual stress introduced by laser peening and cavitation peening depended on the temperature and the peening method. Zhou et al. (2018) commented that the fatigue life depends on the compressive residual stress near the surface and that the strain applied during the fatigue test had an effect on relaxation of the residual stress. Ben Moussa et al. (2019) investigated the improvement in the fatigue life of stainless steel by deep rolling and they also concluded that relaxation of the compressive residual stress depended on the applied strain. Kanou et al. (2012) found that the ratio of the plastic deformation region to dimple depth induced by cavitation peening and laser peening was more than 3 times greater than that induced by conventional shot peening, suggesting that the dislocation density of cavitation and laser peened surfaces are different to conventional shot peened ones. It has also been reported that the introduction of a compressive residual stress, i.e., a macro-strain, by cavitation peening relieves the micro-strain in quenched tool steel alloy, whereas shot peening increases both the micro-and macro-strain (Soyama and Yamada (2008)). Thus, relaxation of the compressive residual stress introduced by cavitation peening might be different from that arising from shot peening.

The stress distribution arising due to the impact by an individual shot is described by Hertz's contact stress equation, and the surface roughness due to shot peening has been investigated (Lin et al. (2019)). On the other hand, Choi and Chahine (2016) attempted to simulate the shape of the pit and plastic strain induced by a single bubble collapsing using fully coupled bubble dynamics and material response, and Sonde et al. (2018) proposed a method to predict the residual stress due to a cloud of bubbles from knowing the distribution of vapor volume fraction in the cavitating flow. However, cavitation bubbles, which are used in cavitation peening, form a cloud consisting of small tiny bubbles and the underlying shapes are longitudinal vortices (Soyama et al. (1995)). Note that a figure in certain studies showed that the vortex cavitation in the shear layer directly produces a ring region, but this is incorrect (Soyama, 2020b). As Reisman et al. (1998) has pointed out, the shock wave induced by cloud cavitation is larger than that due to single bubble cavitation. Therefore, since it is still difficult to simulate the impact due to bubbles collapsing during cavitation peening, experimental studies are still needed to clarify the difference between surfaces treated with conventional shot peening and those treated with cavitation peening.

Odhiambo and Soyama (2003) reported that the fatigue life of shot peened samples was larger than that of cavitation peened samples when the applied stress was relatively high; however, the fatigue strength of cavitation peened carbonized steel samples was greater than that of shot peened samples. They concluded that the surface

roughness and compressive residual stress are important factors for determining the fatigue strength. Note that they also reported that the compressive residual stress distribution introduced by cavitation peening was very shallow compared to that introduced by shot peening. Also, Masaki et al. (2008) measured the residual stress, the 0.2 % proof stress and the hardness using a rotating bending fatigue test to investigate the fatigue properties of shot peened and cavitation peened stainless steel. They concluded that the plastic strain introduced by shot peening was larger than that introduced by cavitation peening and that the fatigue properties corresponded well with the plastic strain. In the case of the treatment of a small round bar by cavitation peening, the peening intensity was insufficient, as most of the cavitation cloud passed through the bar without collapsing. Note that the cavitation system and conditions were optimized to treat a small round bar such as a spinal implant (Takakuwa et al. (2016)). In order to clarify the differences between the various peening methods used for improving the fatigue strength of metallic materials, Soyama (2019) treated individual plane bending fatigue test specimens made of stainless steel at optimum processing times by shot peening, cavitation peening, water jet peening and submerged laser peening. The author reported a similar tendency to that described in a previous report by Odhiambo and Soyama (2003), in which the fatigue life at high applied stress of a shot peened sample was longer than that of a cavitation peened sample, and that the fatigue strength after cavitation peening was greater than that after shot peening. The surface residual stress was measured in the previous paper, however, the residual stress distribution before and after the fatigue test was not evaluated. Thus, it is worth measuring the compressive residual stress introduced by peening both before and after fatigue testing.

There are several ways to evaluate the residual stress in polycrystalline metals. Mechanical methods, such as hole drilling (E837-13a (2013)) and the slitting method (Hill (2013)) are commonly used. Here Lee and Hill (2007) confirmed the repeatability of the slitting method for measuring the residual stress distribution in stainless steel treated by laser peening (Dane et al. (1995)); thus, in the present paper, the slitting method was used to evaluate the variation of residual stress with depth. The other commonly used method to determine the residual stress as a function of depth is X-ray diffraction with electrochemical polishing. Since Soyama (2018) has reported that the residual stress introduced by submerged laser peening measured by the $\sin^2\psi$ and cos α methods are affected by the microstructure, such as the texture of the material, in this present paper, the 2D X-ray diffraction method (He (2009)) was used to evaluate the residual stress.

In this paper, in order to clarify the differences between the material properties of the surface layers modified by cavitation peening and shot peening, stainless steel specimens were treated by cavitation peening and shot

peening, and the properties of these specimens were evaluated using a plane bending fatigue test. The residual stress as a function of depth before and after the fatigue test, the surface roughness and Vickers's surface hardness were also measured. Then, factors related to the fatigue strength were discussed.

2. Experimental Apparatus and Procedure

2.1. Evaluation of fatigue strength and mechanical properties

The fatigue strength and fatigue life of the peened specimens were evaluated by a conventional Schenk-type displacement controlled plate bending fatigue tester at stress ratio $R = -1$ (fully reversed stressing). Note that the maximum applied stress is produced at the surface by the bending moment, which is generated by the displacement. The applied bending moment was monitored by a load cell, and when the bending moment became about 20% of the initial applied bending moment, it was deemed that a failure occurred. Because the bending moment was decreased during the last cycles, as the displacement-controlled plane bending fatigue tester was used at the present study. The comparison between shot peening and cavitation peening by observation of crack initiation and crack growth in stainless steel using a special made load-controlled plane bending fatigue tester was in the reference (Soyama, 2020a). If the specimen was unbroken after $N = 10^7$ cycles, the test was stopped. The fatigue strength at $N = 10^7$ was calculated using a method proposed by Little (1972). The test frequency was 12 Hz. The plane bending fatigue tester is a displacement controlled fatigue tester, so the applied stress σ_a was slightly different in each case. The number of cycles to failure N_f at a certain σ_a is obtained from Eq. (1), so the relationship between N_f and σ_a can be expressed by Eq. (2) with $N_f < 10^6$ (Soyama and Sanders (2019)),

$$N_f = 10^{\frac{c_2 - \sigma_a}{c_1}} \quad (1)$$

$$\sigma_a = -c_1 \log N_f + c_2 \quad (2)$$

Here, c_1 and c_2 are constants, and they were obtained from experimental data by the least-squares method. The variation of N_f was also obtained from c_1 and c_2 of the standard deviation of obtained by the least-squares method.

Figure 1 illustrates the geometry of the specimens used in the plane bending fatigue test, and the geometry was the same as used in a previous study (Soyama, 2019). In order to avoid initiating a crack from the edge, this was rounded with a radius of 0.2 mm by a chamfering tool before peening. The material under test was austenitic stainless steel JIS SUS316L. Tables 1 and 2 show the chemical composition and mechanical properties of this steel. The specimens were made from a plate with a No. 2B surface finish, i.e., done by temper rolling.

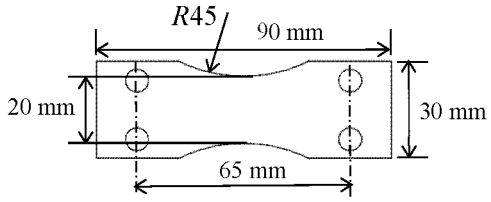

Fig. 1 Dimensions of bending fatigue specimen (Thickness : 2 mm)

Table 1 Chemical composition of the tested stainless steel (mass %)

C	Si	Mn	P	S	Ni	Cr	Mo
0.019	0.70	1.02	0.030	0.002	12.08	17.35	2.07

Table 2 Mechanical properties of the tested stainless steel

Yield strength (0.2 %)	Tensile strength	Elongation
309 MPa	562 MPa	51 %

As one of the major factors related to the fatigue life and strength is residual stress, the residual stress, σ_R, in the longitudinal direction of the specimen was measured by a 2D X-ray diffraction method (He (2009)) and the slitting method Hill (2013) . The X-ray diffraction patterns were obtained using Kα X-rays from a Cr-tube operating at 35 kV and 40 mA through a 0.8 mm diameter collimator with an incident monochromator. The diffraction angle from the γ-Fe (2 2 0) plane without strain was 128 degrees. Twenty four diffraction rings were detected from the specimen at various angles using a two-dimensional detector, considering the conditions used in a previous report by Takakuwa and Soyama (2013). The variation of σ_R with depth beneath the surface, z, was obtained by removing the surface by electrochemical polishing. In the case of the slitting method, slitting was done using a wire electric discharge machine (EDM), and the variation of σ_R with z was evaluated from the strain. A linear strain gage with a gage length of 0.81 mm was bonded to the back of the sample opposite the EDM slit. The gage was waterproofed prior to cutting using silicon sealant. A strain gage on a secondary sample of the same material was used for thermal compensation and placed near the measured sample during cutting. Slitting was performed using a 0.254 mm diameter wire and 17 cut increments of varying depth. These depths increments were 0.0254 mm for 5 increments, 0.0508 mm for 5 increments, and 0.1016 mm for 7 increments. After each cut depth increment the strain was recorded. The variation of σ_R with depth beneath the surface, z, is calculated using the recorded strain and solving an inverse problem following the procedure in Schajer and Prime (2006). In order to consider the plastic deformation

induced by cavitation peening and shot peening, the full width at half maximum, *FWHM*, was also measured using the diffraction ring, which was obtained at each depth simultaneously with the x-ray residual stress measurement.

As the fatigue life and strength of the peened specimens depend on the surface roughness and the hardness, the arithmetic mean roughness, R_a, the maximum height of the roughness, R_z, and the Vickers hardness at the surface, H_V, were measured. The surface roughness was evaluated using a stylus type profilometer. The load used in measuring the Vickers hardness was 0.2 kgf, i.e., 1.96 N. The hardness was measured seven times in each case. The maximum and minimum values were disregarded, and the five remaining values were used to calculate the mean and standard deviation.

2.2. Cavitation peening system

For cavitation peening, cavitation is produced by injecting a high-speed water jet through a nozzle into a water-filled chamber, as shown in Fig. 2. The nozzle consists of a nozzle plate, a cavitator and a guide pipe. The cavitator and guide pipe enhance the aggressive intensity of the cavitating jet. Soyama (2011) has conducted experiments to determine the optimum geometry of the nozzle, and the geometries of the cavitator and the guide pipe have also been optimized by Soyama (2014). The throat dimeter d, and the thickness t_n of the nozzle plate are 2 mm and 6 mm, respectively. The diameter D and length L of the outlet bore are 16 mm and 16 mm, respectively. The diameter of the cavitator, d_c, is 3 mm. The inner diameter and length of the guide pipe are 44 mm and 46 mm, respectively. The injection pressure, p_1, pressurized by a plunger pump is 30 MPa. The standoff distance, s, which is defined as the distance from the upstream edge of the nozzle plate to the surface of the specimen was chosen to be 222 mm, the same as in a previous report ((Soyama (2019)). The depth of the water, where the specimen is placed, is 300 mm.

The processing time per unit length, t_p is defined as follows.

$$t_p = \frac{n}{v} \tag{3}$$

where, n and v are the number of passes and the scanning speed of the nozzle, respectively. For the present experiment, t_p was chosen to be 8 s/mm, the same as in the previous report (Soyama (2019)) in order to minimize the curvature due to peening, the specimen was treated at v = 1 mm/s and n = 8 with turning over the specimen . The cavitation clouds generated by the jet developed as ring vortex cavitation at the sample surface, and then collapsed producing impacts. The specimen was placed in a recess to make the surface flat.

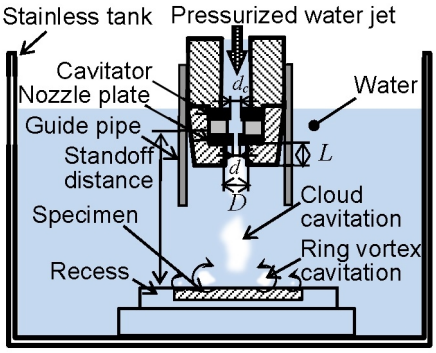

Fig. 2 Schematic diagram of cavitation peening system

2.3. Shot peening system

Figure 3 illustrates a schematic diagram of the shot peening system, which was developed by Naito et al. (2012) and was used in a previous study (Soyama, 2019). In the system, shots are accelerated by a water jet with an injection pressure of 12 MPa through three 0.8 mm diameter holes on a pitch circle diameter (PCD) of 16 mm. For our experiments, stainless steel Japanese Industrial Standards JIS SUS440C shot were used. These recirculate in a chamber with an inner diameter of 54 mm. The standoff distance from the nozzle to the specimen surface was 50 mm. The diameter and number of shot used were 3.2 mm and 500, respectively. Note that no compressive residual stress can be introduced into the stainless steel by the water jet alone under the same conditions. The specimens were treated uniformly by moving the chamber at constant speed. In order to avoid loose shot, the specimen is placed in a recess to make a flat surface, and the chamber is scanned across the surface. The processing time per unit length is defined in the same way as that for cavitation peening (Eq. (3)). In the case of shot peening, t_p was chosen to be 1 s/mm considering the result of a previous report (Soyama (2019)).

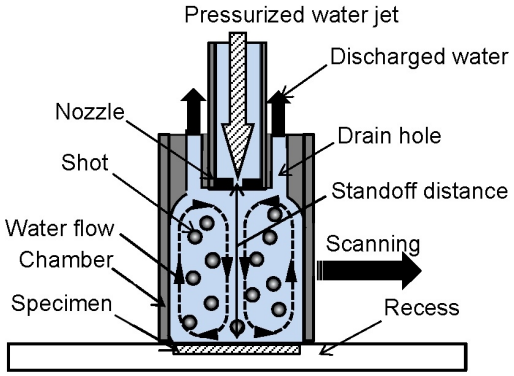

Fig. 3 Schematic diagram of shot peening system

3. Results

3.1. Comparison on the improvement of fatigue properties between cavitation peening and shot peening

In order to clarify the differences between the improvements made to the fatigue life and strength after cavitation peening and shot peening, Fig. 4 shows the relationship between the number of cycles to failure N and the amplitude of the bending stress σ_a obtained from the plane bending fatigue test for cavitation peened, shot peened and non-peened specimens. In Fig. 4, the closed and open symbols signify that the crack starts from the surface and the edge, respectively. Figure 5 shows typical images of cross sectional views of the fractured surfaces of the non-peened, cavitation peened and shot peened specimens. The white arrow in Fig. 5 shows the point from which the crack initiates. As shown in Figs. 4 and 5, at relatively high numbers of cycles to failure, i.e. $N > 7 \times 10^5$, the fracture starts from the edge. Both cavitation peening and shot peening improve the fatigue life and fatigue strength compared with the non-peened specimen, similar to the results reported by Soyama (2019). The fatigue strength at $N = 10^7$ was 266 ± 11 MPa for the non-peened specimen, 345 ± 8 MPa for the cavitation peened specimen and 335 ± 8 MPa for the shot peened specimen. The fatigue life at σ_a = 400 MPa was calculated using Eq. (2). These were $(2.78 \pm 0.29) \times 10^4$ for the non-peened specimen, $(2.74 \pm 0.37) \times 10^5$ for the cavitation peened specimen and $(3.48 \pm 0.26) \times 10^5$ for the shot peened specimen. The difference between the fatigue life for shot peened specimen and cavitation peened specimen was decreased with decrease of σ_a. These results suggest that the fatigue life after shot peening at relatively large σ_a is longer than that of cavitation peening, however, the fatigue strength after cavitation peening is slightly larger than that of shot peening. This tendency is similar to the results given by Soyama (2019).

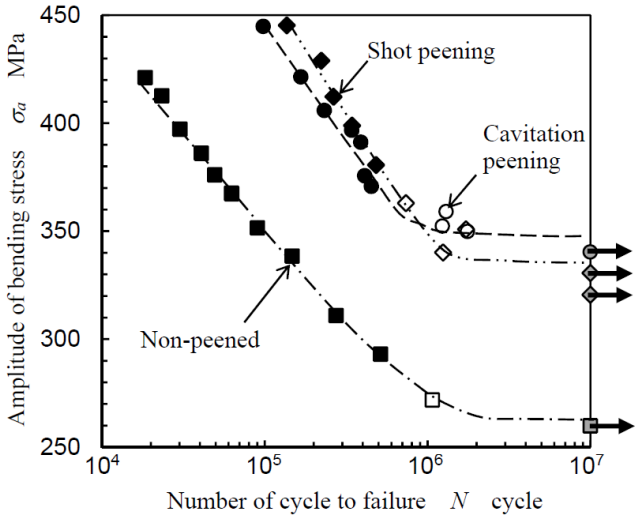

Fig. 4 S-N curves of a non-peened specimen and specimens treated by shot peening and cavitation peening

(a) Non-peened (σ_a = 421 MPa, N_f = 1.85×10^4)

(b) Non-peened (σ_a = 272 MPa, N_f = 1.07×10^6)

(c) Cavitation peening (σ_a = 445 MPa, N_f = 9.81×10^4)

(d) Cavitation peening (σ_a = 352 MPa, N_f = 1.23×10^6)

(e) Shot peening (σ_a = 445 MPa, N_f = 1.37×10^5)

(f) Shot peening (σ_a = 340 MPa, N_f = 1.24×10^6)

Fig. 5 Aspects of the fractured surfaces

In order to investigate why the fatigue strength after shot peening was lower than that after cavitation peening, Fig. 6 shows images of the surfaces and edges of non-peened, cavitation peened and shot peened specimens. Figure 6 was obtained by stacking the images, which were observed at an angle of about 45 degrees to the surface with a colormap of height along the 45 degree axis, by using a digital microscope. In Fig. 6, the surface of the specimen subjected to peening is on the upper right hand side. As can be seen in Fig. 6, the edge of the non-peened specimen was rounded with a radius of 0.2 μm using a chamfering tool. In the case of cavitation peening, plastic deformation pits can be seen on the peened surface and a few pits can be seen on the edge. On the other hand, in the case of shot peening, the deformation at the edge is remarkable compared with cavitation peening. This plastic deformation would lead to cracks at lower applied stress compared with cavitation peening.

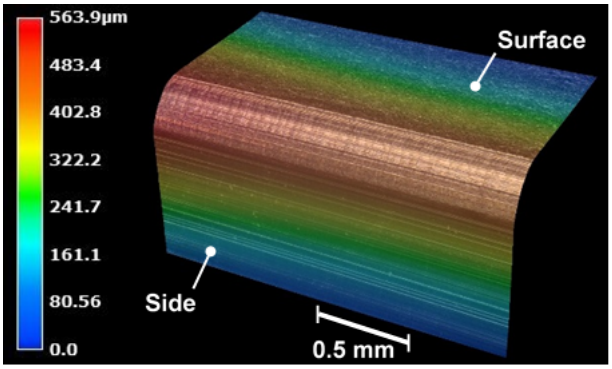

(a) Non-peened

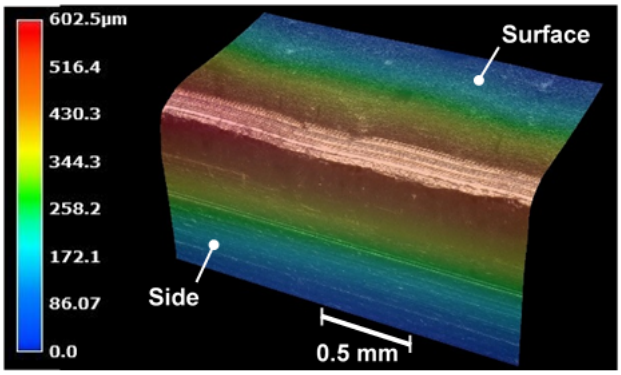

(b) Cavitation peening

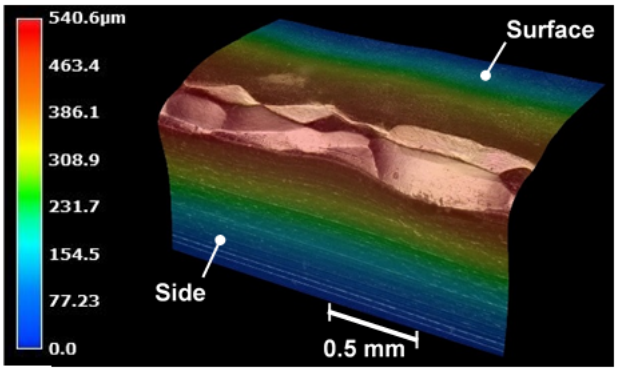

(c) Shot peening

Fig. 6 Aspects of edges of the different specimens

3.2. Comparison between the mechanical properties of the surfaces after cavitation peening and shot peening

In order to determine the reason why the fatigue strength after shot peening was smaller than that after cavitation peening, even though the fatigue life at σ_a = 400 MPa after shot peening was longer than that after cavitation peening, the variation in residual stress, σ_R, with depth, z, was measured. The residual stress in non-peened (NP), cavitation peened (CP) and shot peened (SP) specimens before and after the fatigue test is shown in

Figs. 7 and 8. The measurements in Fig. 7 were made using the 2D X-ray diffraction method while those in Fig. 8 were made using the slitting method. The numbers following NP, CP and SP refer to the applied stress σ_a and the number of cycles in the fatigue test. For example, NP0 and CP350-100 mean non-peened without a fatigue test and cavitation peened after a fatigue test of 100 cycles with σ_a = 350 MPa, respectively.

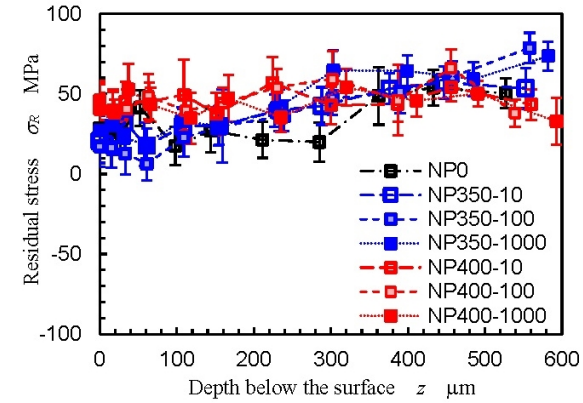

(a) Non-peened

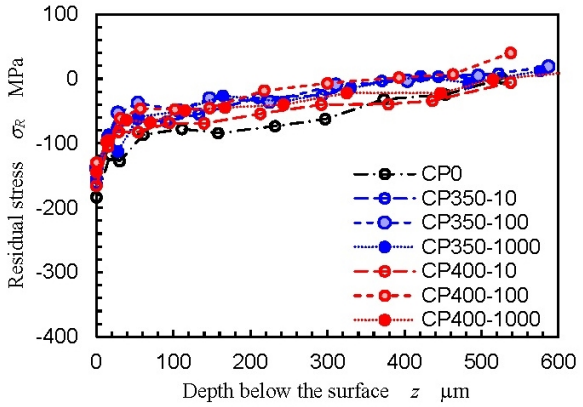

(b) Cavitation peening

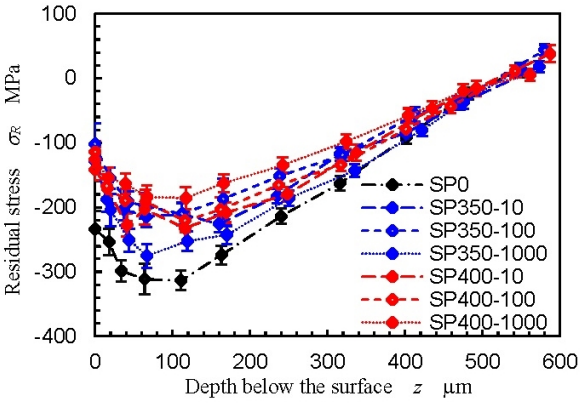

(c) Shot peening

Fig. 7 Residual stress measured by the 2D X-ray diffraction method as a function of depth below the surface

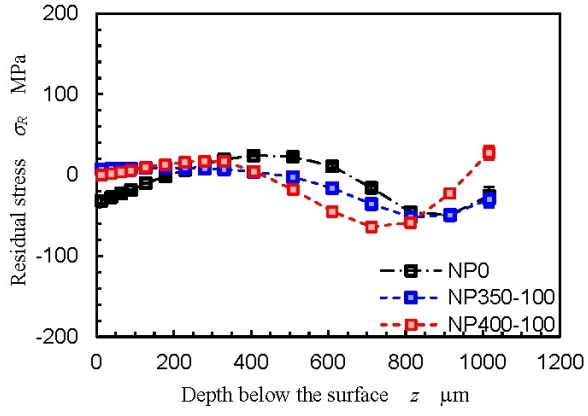

(a) Non-peened

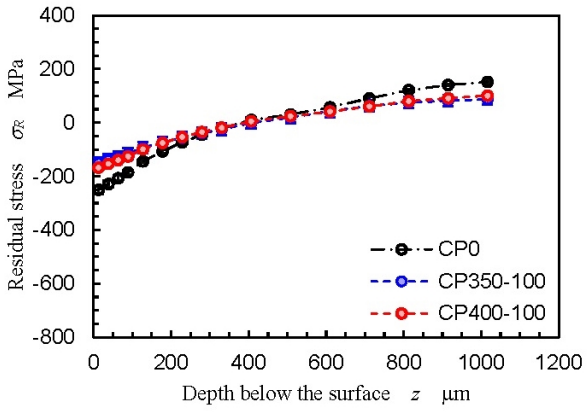

(b) Cavitation peening

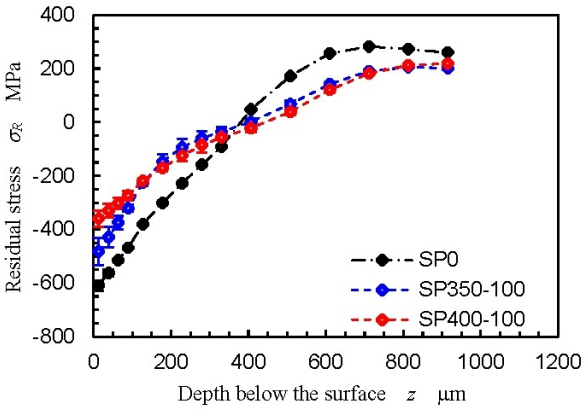

(c) Shot peening

Fig. 8 Residual stress measured by the slitting method as a function of depth below the surface

As shown in Figs. 7 and 8, compressive residual stress was introduced by both cavitation peening and shot peening. The compressive residual stress decreased after the fatigue test as reported by Zhou et al. (2018). The reduction in stress was more remarkable when the applied stress was larger and/or the number of cycles was

greater. Even for the non-peened specimen, the residual stress became more tensile.

If we compare the residual stress at the surface measured by the 2D X-ray diffraction method, we can see that this is almost the same for cavitation peening and shot peening, with $\sigma_R \approx$ -200 MPa. After the fatigue test, however, the residual stress at the surface of the shot peened specimens is reduced by $\Delta\sigma_R \approx$ 150 MPa, whereas the reduction in the cavitation peened specimens is $\Delta\sigma_R \approx$ 50 MPa. Note that the maximum compressive residual stress beneath the surface in the shot peened specimens occurs at z = 50 – 100 μm. This residual stress is greater than that introduced by cavitation peening, and even after fatigue tests at σ_a = 350 MPa and 400 MPa the maximum residual stress in the shot peened specimens is greater than that in the cavitation peened specimens. For example, σ_R for SP400-1000 at z = 67 μm and CP400-1000 at z = 70 μm are -184 ± 18 MPa and -68 ± 10 MPa, respectively.

As shown in Fig. 8, in the case of measurements by the slitting method, the compressive residual stress after shot peening is larger than that after cavitation peening at any depth, both before and after the fatigue test. Figure 8 also shows that the residual stress at the surface of the shot peened specimens after the fatigue test is reduced by $\Delta\sigma_R \approx$ 250 MPa, which is greater than the reduction, $\Delta\sigma_R \approx$ 80 MPa, in the cavitation peened specimens. For example, before the fatigue test, at z = 13 μm, σ_R in the shot peened and cavitation peened specimens are -609 ± 19 MPa and -251 ± 16 MPa, respectively. After a fatigue test of 100 cycles with σ_a = 400 MPa, σ_R in the shot peened and cavitation peened specimens are -359 ± 30 MPa and -168 ± 7 MPa, respectively.

Comparing the results from these two measurement methods, the tendencies and values of the non-peened and cavitation peened specimens are roughly similar. However, in the case of shot peening, the residual stresses measured by the 2D X-ray diffraction method and the slitting method are different, especially beneath the surface. In the case of the 2D X-ray diffraction method, the maximum compressive residual stress is at z = 50 – 100 μm, and the stress near the surface is lower. On the other hand, σ_R for SP0 at z = 13 μm measured by the slitting method is -609 ± 19 MPa, and σ_R for SP0 at z = 18 μm measured by the 2D X-ray diffraction method is -254 ± 21 MPa. That is, the maximum compressive residual stress measured by the slitting method is near the surface, and this value is greater than the stress at the surface measured by the 2D X-ray diffraction method.

Considering the results from both of these methods, it was concluded that the compressive residual stress introduced into the stainless steel by shot peening is greater and goes deeper compared with cavitation peening. Also, the reduction in residual stress after the fatigue test was greater for shot peening than for cavitation peening.

In order to investigate the plastic characteristics introduced by cavitation peening and shot peening, the full

width at half maximum, *FWHM*, of the X-ray diffraction patterns as a function of depth, *z*, below the surface for specimens before and after the fatigue test are plotted in Fig. 9. The *FWHM* for both cavitation peened and shot peened samples is at its maximum at the surface, and decreases with *z*. The *FWHM* also decreases after the fatigue test, just like the compressive residual stress discussed above. In the case of cavitation peening, the *FWHM* at the surface decreases from 0.78 ± 0.02 deg. before the fatigue test to 0.75 ± 0.02 deg. after the fatigue test. On the other hand, in the case of shot peening, the *FWHM* decreases from 0.98 ± 0.02 deg. to 0.88 ± 0.04 deg. after the fatigue test. Thus, the *FWHM* for shot peening is greater than that for cavitation peening, and also the decrease in *FWHM* for shot peening is more than that for cavitation peening. As the *FWHM* indicates a kind of lattice strain in the grain, the plastic strain introduced by shot peening is greater than that introduced by cavitation peening at $z <$ 400 μm.

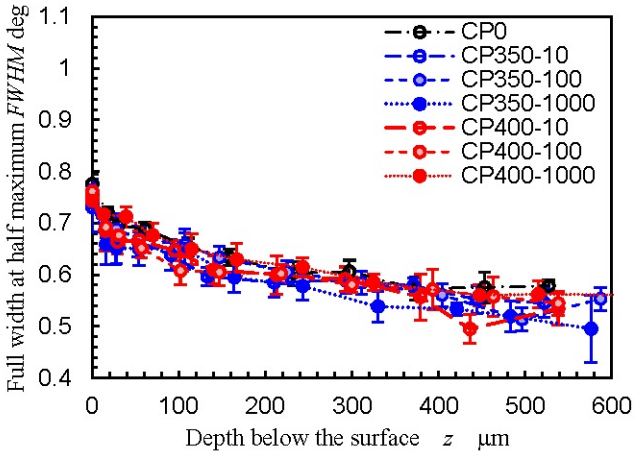

(a) Cavitation peening

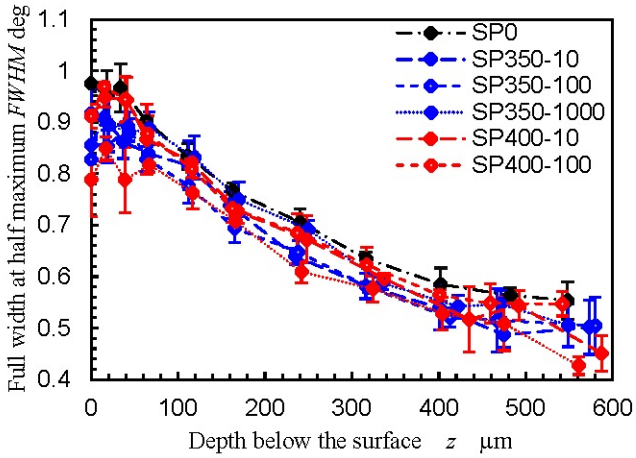

(b) Shot peening

Fig. 9 Full width at half maximum of X-ray diffraction as a function of depth below the surface

The local plastic deformation caused by the peening methods introduces compressive residual stress. To investigate the relationship between the plastic deformation and the residual stress, we examined the relationships between the residual stress and the *FWHM*. Plots of these are shown in Fig. 10 for both shot peened and cavitation peened specimens. The residual stresses measured by the 2D X-ray diffraction method and the slitting method are plotted in Fig. 10 (a) and Fig. 10 (b), respectively. As shown in Fig. 10 (a) and (b), the compressive residual stress decreases as the *FWHM* decreases. In the case of Fig. 10 (a), the data points for cavitation peening and shot peening lie on two separate sets of curves. Also, the curves for the shot peened samples at higher *FWHM* plateau due to the residual stress data beneath the surface. On the other hand, in Fig. 10 (b), the data points are roughly on the same set of curves for both cavitation peening and shot peening. Thus, the residual stress measurements made by the slitting method are used in the discussion below (Section 4).

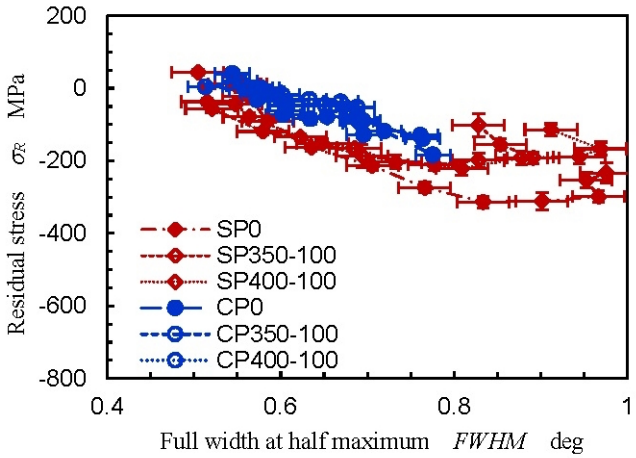

(a) Residual stress measured by the 2D X-ray diffraction method

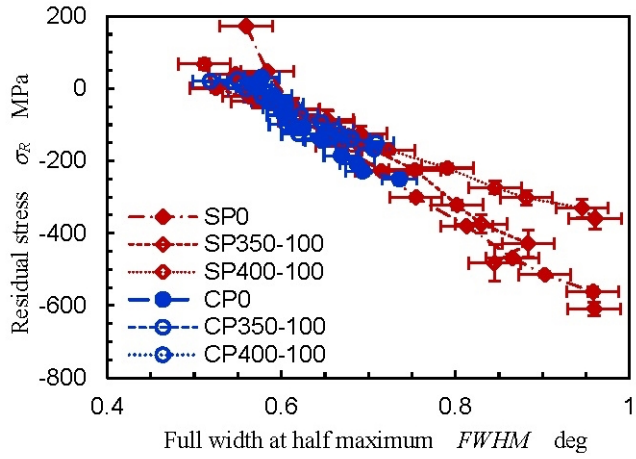

(b) Residual stress measured by the slitting method

Fig. 10 Relationship between the full width at half maximum of the X-ray diffraction profile and residual stress

As the hardness and the surface roughness also affect the fatigue life and strength, Figs. 11 and 12 show the Vickers hardness and the surface roughness. As shown in Fig. 11, the Vickers hardness after cavitation peeing and shot peening before the fatigue test were 240 ± 6 and 273 ± 7, respectively. These are increases by factors of about 1.5 and 1.7 compared with the non-peened specimen, i.e., 160 ± 5. The increase in the Vickers hardness after shot peening is about 14 % greater than that after cavitation peening. Note that the Vickers hardness for the cavitation peened, shot peened and non-peened specimens decrease slightly after the fatigue test. As shown in Fig. 12, the arithmetic mean roughness R_a and the maximum height of the roughness R_z increased by factors of between 10 and 20 after cavitation peening and shot peening. The R_a and R_z of the non-peened specimen were 0.05 ± 0.03 μm and 0.45 ± 0.21 μm, respectively. The values of R_a and R_z after shot peening were about 26 % and 28 % greater than those after cavitation peening, respectively. Thus, with regard to the fatigue strength, it seems that the higher surface roughness of the shot peened specimens compared to that of the cavitation peened specimens cancels the advantages of the greater Vickers hardness of the shot peened specimens.

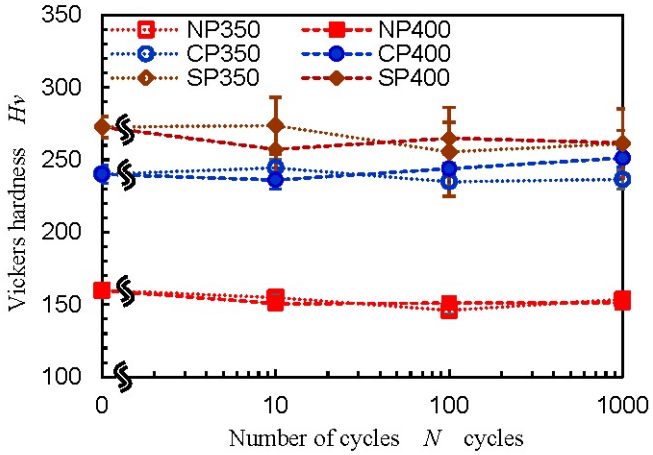

Fig. 11 Variation of Vickers hardness with the number of cycles

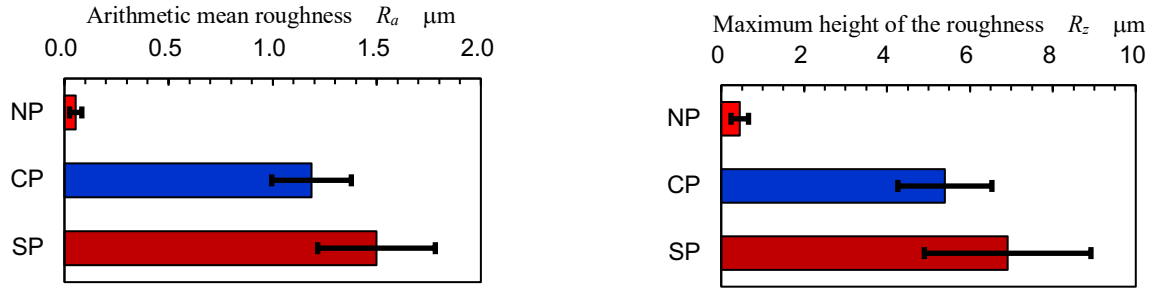

(a) Arithmetic mean roughness R_a (b) Maximum height of the roughness R_z

Fig. 12 Surface roughness

4. Discussion

Masaki et al. (1999) sought to explain the improvement in fatigue strength by shot peening considering the hardness and roughness. They (Masaki et al. (1999)) discussed the effect of surface roughness on the improvement in fatigue strength of austenitic stainless steel by hard shot peening using the $\sqrt{area}$ parameter proposed by Murakami et al. (1997) (see Eq. (4)), and concluded that the effect of hard shot peening could not be described using the $\sqrt{area}$ parameter.

$$\sigma_w = 1.43(H_V + 120)/(\sqrt{area})^{\frac{1}{6}} \quad (4)$$

Here, σ_w is the fatigue strength estimated using the $\sqrt{area}$ parameter.

In our experiment, when R_z was used for the $\sqrt{area}$ parameter, σ_w was calculated to be 457 MPa for the non-peened sample, 389 MPa for the cavitation peened sample and 388 MPa for the shot peened sample. Thus, we also conclude, in agreement with Masaki et al. (1999), that the improvement in σ_w by peening cannot be explained using the $\sqrt{area}$ parameter.

Regarding Eq. (4), the most important factor is the hardness. As shown experimentally by Takakuwa et al. (2013), the compressive residual stress without work hardening increases the Vickers hardness. That is, the Vickers hardness takes into account both the yield stress and the compressive residual stress. In the present paper, since the yield stress is closely related to the fatigue life and strength, we discuss the relationship between the fatigue strength and the yield stress, which is obtained from the Vickers hardness taking into account the residual stress.

Table 3 shows the yield stress σ_y estimated from the Vickers hardness H_V corrected for residual stress. Takakuwa et al. (2013) proposed an equation based on experimental results to estimate the yield stress $\sigma_{y\,est}$ of austenitic stainless steel SUS316L from the Vickers hardness corrected for residual stress, H_V':

$$H_V' = H_V + (8.4 \pm 1.4) \times 10^{-2}\sigma_R \quad (5)$$

$$\sigma_{y\,est} = (3.32 \pm 1.8)H_V' - (218 \pm 30) \quad (6)$$

where σ_R is the residual stress in MPa. Note that the value of $\sigma_{y\,est}$ without a fatigue test, 304 ± 44 MPa, corresponds well with the yield strength given in Table 2, i.e., 309 MPa. As mentioned above, the values measured by the slitting method were used for σ_R in Table 3. As the fatigue limit of steels can be simply estimated by 1.6 H_V on the basis of empirical rule (Murakami, 2012) , the estimated fatigue strength $\sigma_{f\,est}$ and $\sigma_{f\,est}$' from H_V and H_V' are shown in Table 3.

Table 3 Estimation of yield stress and fatigue strength from Vickers hardness corrected by residual stress

	Residual stress σ_R MPa	Vickers hardness H_V	Corrected Vickers hardness H_V'	Estimated yield stress $\sigma_{y\,est}$ MPa	Estimated fatigue strength from H_V $\sigma_{f\,est}$ MPa	Estimated fatigue strength from H_V' $\sigma_{f\,est}$' MPa
NP0	-32 ± 3	160 ± 5	157 ± 5	304 ± 44	256 ± 8	251 ± 8
NP350-100	7 ± 2	146 ± 3	147 ± 2	269 ± 41	234 ± 5	235 ± 3
NP400-100	0 ± 3	151 ± 3	151 ± 2	283 ± 42	242 ± 5	242 ± 3
CP0	-252 ± 16	240 ± 6	219 ± 7	509 ± 55	384 ± 10	350 ± 11
CP350-100	-151 ± 5	235 ± 4	222 ± 4	519 ± 52	376 ± 6	355 ± 6
CP400-100	-168 ± 7	244 ± 14	230 ± 14	545 ± 70	390 ± 22	368 ± 22
SP0	-609 ± 19	273 ± 7	221 ± 11	517 ± 62	437 ± 11	354 ± 18
SP350-100	-483 ± 50	255 ± 31	215 ± 32	495 ± 116	408 ± 50	344 ± 51
SP400-100	-359 ± 30	265 ± 11	235 ± 13	561 ± 66	424 ± 18	376 ± 21

Figure 13 shows the relationship between the estimated yield stress, $\sigma_{y\,est}$, calculated from Eq. (6), and the fatigue strength, σ_f, measured by the current tests. This shows that σ_f is proportional to $\sigma_{y\,est}$. For the specimens after fatigue tests of 100 cycles at σ_a = 350 MPa, the correlation coefficient is 0.999 and the probability of no correlation is 1.42 %. As this is less than 5 %, it can be concluded that the relationship between $\sigma_{y\,est}$ and σ_f is significant. From the present result, the following relationship between σ_f and $\sigma_{y\,est}$ was obtained.

$$\sigma_f = (0.311 \pm 0.009)\,\sigma_{y\,est} - (182 \pm 4) \qquad (7)$$

In the case of the specimens after fatigue tests of 100 cycles at σ_a = 400 MPa and the specimens that had not had fatigue tests, the probability of no correlation is 13 % and 12 %, respectively. With σ_a = 400 MPa, the applied stress was too large as the yield strength was about 300 MPa. Thus, in order to obtain the yield stress related to the fatigue strength, the reduction in compressive residual stress near the fatigue strength should be considered.

Figure 14 shows the relation between corrected Vickers hardness H_V' and fatigue strength σ_f with the line of σ_f = 1.6 H_V'. The correlation coefficient between H_V' and σ_f is 0.927 for σ_R without fatigue test, 0.833 for σ_R after fatigue tests of 100 cycles at σ_a = 350 MPa and 0.709 for σ_R after fatigue tests of 100 cycles at σ_a = 400 MPa. It can be concluded that the fatigue strength can be roughly estimated from the corrected Vickers hardness H_V', however, the correlation coefficient between σ_f and $\sigma_{y\,est}$ using Eq. (7) is larger than that of H_V' and σ_f. For both cases, the surface residual stress and the surface Vickers hardness were used for the estimation of the fatigue

strength. Namely, the fatigue strength depends on the surface residual stress and the surface Vickers hardness. This tendency is consistent with the result that the surface residual stress and the surface Vickers hardness had good correlation with the threshold stress intensity factor range ΔK_{th}, which was obtained by a K-decreasing test using a load-controlled plane bending fatigue tester (Soyama, 2020a).

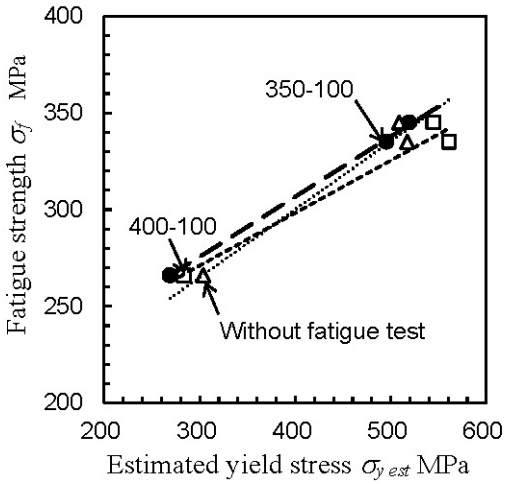

Fig.13 Relationship between estimated yield stress, $\sigma_{y\,est}$, and fatigue strength, σ_f.

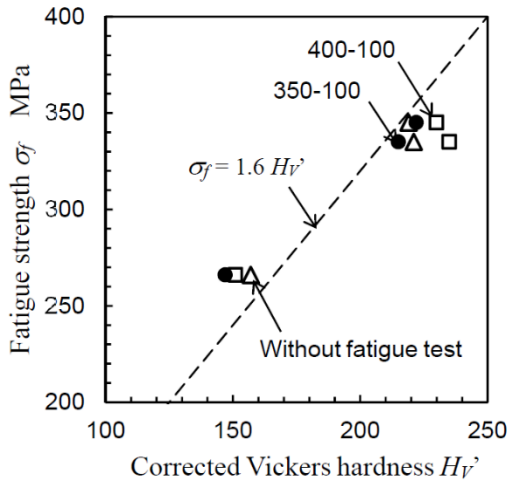

Fig. 14 Relation between corrected Vickers hardness H_V' and fatigue strength σ_f

5. Conclusions

In order to clear the main factor on the improvements of the fatigue life and fatigue strength of metallic materials by cavitation peening and shot peening, the fatigue properties of peened samples were evaluated by a

plane bending fatigue test. And compressive residual stress introduced by peening in austenitic stainless steel JIS SUS316L was measured considering the reduction in residual stress resulting from the fatigue test. The residual stress was measured by a 2D X-ray diffraction method and a slitting method. The results obtained for the material under test, austenitic stainless steel JIS SUS316L, can be summarized as follows.

(1) Both cavitation peening and shot peening increased the fatigue life and fatigue strength of specimens compared with a non-peened specimen. The improvements after both cavitation peening and shot peening were roughly the same, however, the compressive residual stress introduced by shot peening was greater and deeper compared to that introduced by cavitation peening.

(2) When the residual stresses measured by the 2D X-ray diffraction method and the slitting method were compared, these were roughly similar for the non-peened and cavitation peened specimens. On the other hand, in the case of shot peening, the compressive residual stress beneath the surface measured by the slitting method was two or three times larger than that given by the 2D X-ray diffraction method.

(3) As the relationship between the plastic deformation evaluated from the full width at half maximum and the residual stress measured by the slitting method is the same for both shot peening and cavitation peening, the residual stress beneath the surface of the shot peened specimen measured by the slitting method is reasonable.

(4) The reduction in compressive residual stress during the plane bending fatigue test of the shot peened specimen was remarkable compared with that of the cavitation peened specimen. That is, the reduction in compressive residual stress during the fatigue test of the cavitation peened specimen was small. Note that the residual stress of the non-peened specimen became more tensile after the fatigue test.

(5) There was good correlation between the fatigue strength and the yield stress estimated from the Vickers hardness corrected by the residual stress measured by the slitting method, considering the reduction in residual stress after the fatigue test.

(6) The fatigue strength at $N = 10^7$ was 266 ± 11 MPa for the non-peened specimen, 345 ± 8 MPa for the cavitation peened specimen and 335 ± 8 MPa for the shot peened specimen, respectively. As shot are not used in cavitation peening, the edges were scarcely deformed, thus the fatigue strength of the cavitation peened specimens was slightly larger than those of the shot peened specimens.

Acknowledgements

This work was partly supported by JSPS KAKENHI Grant Number 17H03138, 18KK0103 and 20H02021.

The authors wish to thank Mr. M. Kobayashi, administrative assistant of the Department of Finemechanics, Tohoku University for his help in the experiments.

Reference

Bagherifard, S., Ghelichi, R. and Guagliano, M., 2012. Numerical and experimental analysis of surface roughness generated by shot peening, Applied Surface Science, 258 (18), 6831-6840, 10.1016/j.apsusc.2012.03.111.

Bellows, G. and Koster, W. P. (1972). *Surface integrity - update '72*: General Electric Company.

Ben Moussa, N., Gharbi, K., Chaieb, I. and Ben Fredj, N., 2019. Improvement of aisi 304 austenitic stainless steel low-cycle fatigue life by initial and intermittent deep rolling, International Journal of Advanced Manufacturing Technology, 101 (1-4), 435-449, 10.1007/s00170-018-2955-0.

Choi, J. K. and Chahine, G. L., 2016. Relationship between material pitting and cavitation field impulsive pressures, Wear, 352-353 42-53, 10.1016/j.wear.2016.01.019.

Dane, C. B., Zapata, L. E., Neuman, W. A., Norton, M. A. and Hackel, L. A., 1995. Design and operation of a 150-w near diffraction-limited laser-amplifier with sbs wave-front correction, IEEE Journal of Quantum Electronics, 31 (1), 148-163, 10.1109/3.341719.

Delosrios, E. R., Walley, A., Milan, M. T. and Hammersley, G., 1995. Fatigue-crack initiation and propagation on shot-peened surfaces in a316 stainless-steel, International Journal of Fatigue, 17 (7), 493-499, 10.1016/0142-1123(95)00044-t.

E837-13a, 2013. Standard test method for determining residual stresses by the hole-drilling strain-gage method, ASTM standard, 03.01 1-16, 10.1520/E0837.

Foss, B. J., Gray, S., Hardy, M. C., Stekovic, S., McPhail, D. S. and Shollock, B. A., 2013. Analysis of shot-peening and residual stress relaxation in the nickel-based superalloy rr1000, Acta Materialia, 61 (7), 2548-2559, 10.1016/j.actamat.2013.01.031.

He, B. B., 2009. Two-dimensional X-ray diffraction, John Wiley & Sons, Inc., New Jersey 249-328.

Hill, M., 2013. The slitting method, Practical Residual Stress Measurement Methods 89-108, 10.1002/9781118402832.ch4|.

Kanou, S., Takakuwa, O., Mannava, S. R., Qian, D., Vasudevan, V. K. and Soyama, H., 2012. Effect of the impact energy of various peening techniques on the induced plastic deformation region, Journal of Materials Processing Technology, 212 (10), 1998-2006, 10.1016/j.jmatprotec.2012.05.003.

Kumagai, N., Takakuwa, O. and Soyama, H., 2016. Improvement of delayed fracture resistance on chrome molybdenum steel bolt by cavitation peening, Bulletin of the JSME, 82, paper No. 16-00111, 10.1299/transjsme.16-00111.

Lee, M. J. and Hill, M. R., 2007. Intralaboratory repeatability of residual stress determined by the slitting method, Experimental Mechanics, 47 (6), 745-752, 10.1007/s11340-007-9085-1.

Leverant, G. R., Langer, B. S., Yuen, A. and Hopkins, S. W., 1979. Surface residual-stresses, surface-topography and the fatigue behavior of ti-6al-4v, Metallurgical Transactions a-Physical Metallurgy and Materials Science, 10 (2), 251-257, 10.1007/bf02817635.

Lin, Q. J., Liu, H. J., Zhu, C. C. and Parker, R. G., 2019. Investigation on the effect of shot peening coverage on the surface integrity, Applied Surface Science, 489 66-72, 10.1016/j.apsusc.2019.05.281.

Little, R. E., 1972. Estimating the median fatigue limit for very small up-and-down quantal response tests and for s-n data with runouts, ASTM STP, 511 29-42.

Masaki, K., Tohmyoh, Y., Ochi, Y. and Matsumura, T., 1999. The effect of hard shot-peening on high cycle fatigue properties of sus 316L steel : Evaluation of surface roughness effects using the annealing method, Transaction of the JSME, 65A (630), 334-339.

Masaki, K., Ochi, Y. and Soyama, H., 2008. Fatigue property improvement of type 316L steel by cavitation shotless peening, Proceeding of 10th International Conference on Shot Peening paper No. 053.

McClung, R. C., 2007. A literature survey on the stability and significance of residual stresses during fatigue, Fatigue & Fracture of Engineering Materials & Structures, 30 (3), 173-205, 10.1111/j.1460-2695.2007.01102.x.

Miao, H. Y., Demers, D., Larose, S., Perron, C. and Levesque, M., 2010. Experimental study of shot peening and stress peen forming, Journal of Materials Processing Technology, 210 (15), 2089-2102, 10.1016/j.jmatprotec.2010.07.016.

Munoz-Cubillos, J., Coronado, J. J. and Rodriguez, S. A., 2017. Deep rolling effect on fatigue behavior of austenitic stainless steels, International Journal of Fatigue, 95 120-131, 10.1016/j.ijfatigue.2016.10.008.

Murakami, Y., 2012. Material defects as the basis of fatigue design. International Journal of Fatigue, 41 2-10, 10.1016/j.ijfatigue.2011.12.001.

Murakami, Y., Takahashi, K. and Yamashita, T., 1997. Quantitative evaluation of the effect of surface roughness on fatigue strength : Effect of depth and pitch of roughness, Transaction of the JSME, 63 (612), 1612-1619.

Naito, A., Takakuwa, O. and Soyama, H., 2012. Development of peening technique using recirculating shot accelerated

by water jet, Materials Science and Technology, 28 (2), 234-239, 10.1179/1743284711y.0000000027.

Odhiambo, D. and Soyama, H., 2003. Cavitation shotless peening for improvement of fatigue strength of carbonized steel, International Journal of Fatigue, 25 (9-11), 1217-1222, 10.1016/s0142-1123(03)00121-x.

Reisman, G. E., Wang, Y. C. and Brennen, C. E., 1998. Observations of shock waves in cloud cavitation, Journal of Fluid Mechanics, 355 255-283, 10.1017/s0022112097007830.

Schajer, G. S. and Prime, M. B., 2006. Use of inverse solutions for residual stress measurements, Journal of Engineering Materials and Technology-Transactions of the Asme, 128 (3), 375-382, 10.1115/1.2204952.

Sonde, E., Chaise, T., Boisson, N. and Nelias, D., 2018. Modeling of cavitation peening: Jet, bubble growth and collapse, micro-jet and residual stresses, Journal of Materials Processing Technology, 262 479-491, 10.1016/j.jmatprotec.2018.07.023.

Soyama, H., Yamauchi, Y., Adachi, Y., Sato, K., Shindo, T. and Oba, R., 1995. High-speed observations of the cavitation cloud around a high-speed submerged water-jet, JSME International Journal, 38B (2), 245-251.

Soyama, H. and Yamada, N., 2008. Relieving micro-strain by introducing macro-strain in a polycrystalline metal surface by cavitation shotless peening, Materials Letters, 62 (20), 3564-3566, 10.1016/j.matlet.2008.03.055.

Soyama, H. and Sekine, Y., 2010. Sustainable surface modification using cavitation impact for enhancing fatigue strength demonstrated by a power circulating-type gear tester, International Journal of Sustainable Engineering, 3 (1), 25-32, 10.1080/19397030903395174.

Soyama, H., 2011. Enhancing the aggressive intensity of a cavitating jet by means of the nozzle outlet geometry, Journal of Fluids Engineering, 133, paper No. 101301 (10), 1-11, 10.1115/1.4004905.

Soyama, H., 2014. Enhancing the aggressive intensity of a cavitating jet by introducing a cavitator and a guide pipe, Journal of Fluid Science and Technology, 9, paper No. 13-00238 (1), 1-12, 10.1299/jfst.2014jfst0001.

Soyama, H., 2017. Key factors and applications of cavitation peening, International Journal of Peening Science and Technology, 1 (1), 3-60.

Soyama, H., 2018. Comparison of various XRD methods on evaluation of residual stress introduced by submerged laser peening, Metal Finishing News, 19 (5), 54-57.

Soyama, H., 2019. Comparison between the improvements made to the fatigue strength of stainless steel by cavitation peening, water jet peening, shot peening and laser peening, Journal of Materials Processing Technology, 269 65-78.

Soyama, H. and Sanders, D., 2019. Use of an abrasive water cavitating jet and peening process to improve the fatigue

strength of titanium alloy 6Al-4V manufactured by the electron beam powder bed melting (EBPB) additive manufacturing method Jom, 71 (12), 4311-4318.

Soyama, H., 2020a. Comparison between shot peening, cavitation peening and laser peening by observation of crack initiation and crack growth in stainless steel, Metals, 10 (1), 10.3390/met10010063.

Soyama, H., 2020b. Cavitation peening : a review, Metals, 10 (2), 10.3390/met10020270.

Takakuwa, O. and Soyama, H., 2013. Optimizing the conditions for residual stress measurement using a two-dimensional XRD method with specimen oscillation, Advances in Materials Physics and Chemistry, 03 (01), 8-18, 10.4236/ampc.2013.31A002.

Takakuwa, O., Kawaragi, Y. and Soyama, H., 2013. Estimation of the yield stress of stainless steel from the vickers hardness taking account of the residual stress, Journal of Surface Engineered Materials and Advanced Technology, 3 262-268, 10.4236/jsemat.2013.34035.

Takakuwa, O., Nakai, M., Narita, K., Niinomi, M., Hasegawa, K. and Soyama, H., 2016. Enhancing the durability of spinal implant fixture applications made of Ti-6Al-4V ELI by means of cavitation peening, International Journal of Fatigue, 92 360-367.

Takakuwa, O. and Soyama, H., 2012. Suppression of hydrogen-assisted fatigue crack growth in austenitic stainless steel by cavitation peening, International Journal of Hydrogen Energy, 37, 5286-5276, 10.1016/j.ijhydene.2011.12.035.

Telang, A., Gnaupel-Herold, T., Gill, A. and Vasudevan, V. K., 2018. Effect of applied stress and temperature on residual stresses induced by peening surface treatments in alloy 600, Journal of Materials Engineering and Performance, 27 (6), 2796-2804, 10.1007/s11665-018-3371-1.

Torres, M. A. S. and Voorwald, H. J. C., 2002. An evaluation of shot peening, residual stress and stress relaxation on the fatigue life of aisi 4340 steel, International Journal of Fatigue, 24 (8), 877-886, 10.1016/s0142-1123(01)00205-5.

Wang, S. P., Li, Y. J., Yao, M. and Wang, R. Z., 1998. Compressive residual stress introduced by shot peening, Journal of Materials Processing Technology, 73 (1-3), 64-73, 10.1016/s0924-0136(97)00213-6.

Zhou, J., Retraint, D., Sun, Z. and Kanoute, P., 2018. Comparative study of the effects of surface mechanical attrition treatment and conventional shot peening on low cycle fatigue of a 316L stainless steel, Surface & Coatings Technology, 349 556-566, 10.1016/j.surfcoat.2018.06.041.